ELSEVIER

Polymer 41 (2000) 6627–6634

polymer

Ion selectivity and water dissociation in polymer bipolar membranes studied by membrane potential and current–voltage measurements

A. Alcaraz[a], P. Ramírez[a], S. Mafé[b,*], H. Holdik[c], B. Bauer[d]

[a]*Departament de Ciències Experimentals, Universitat Jaume I, Apdo. 224, E-12080 Castelló, Spain*
[b]*Departament de Termodinàmica, Universitat de València, E-46100 Burjassot, Spain*
[c]*Institut für Prozesstechnik, Universität des Saarlandes, D-66123 Saarbrücken, Germany*
[d]*FuMA-Tech GmbH, Am Grubenstollen 11, Postfach 1327, D-66363 St. Ingbert, Germany*

Received 21 May 1999; received in revised form 23 November 1999; accepted 8 December 1999

Abstract

A polymer bipolar ion-exchange membrane consists of a layered structure involving one cation and one anion ion-exchange layer joined together in series. In this study, the ionic selectivity and water dissociation rate of six commercial bipolar membranes was evaluated from the measurements of the membrane potential in a concentration cell and the current–voltage curve in a four-point measuring cell. Bipolar membrane technology requires polymer membranes presenting high ion selectivities and water dissociation rates, and in this paper we have addressed the basic physico-chemical phenomena involved, both theoretically and experimentally. We have shown that the effects of the bipolar junction and the membrane fixed charge concentrations on the ion transport rates observed can be understood on the basis of simple concepts. © 2000 Elsevier Science Ltd. All rights reserved.

Keywords: Polymer bipolar ion-exchange membranes; Ion transport and water dissociation; Membrane potential and current–voltage measurements

1. Introduction

A polymer bipolar ion-exchange membrane (BM) is composed of one cation and one anion ion-exchange layer joined together in series. This particular arrangement shows high ionic selectivity and its most noticeable characteristic is the electric field enhanced (EFE) water dissociation that occurs at the bipolar junction of the membrane when a high dc electric current is forced through this junction [1–6]. The capability of the system to dissociate water makes it suitable for a large variety of applications, such as generation and recovery of acids and bases [7–10] and the chemical processing of effluents resulting from organic chemistry and biochemistry processes [11–14].

A BM separating two solutions of the same electrolyte at concentrations c_L (left compartment) and c_R (right compartment) is shown schematically in Fig. 1. Under forward electrical polarisation, the current flows from the right solution to the left solution and the salt ions accumulate at the bipolar junction (see Fig. 1). In reverse electrical polarisation, these ions are pulled out from the junction [4]. The H^+ and OH^- ions are then assumed to be generated at the interfacial region between the two ion-exchange layers within the depleted space charge region extending from $x = -\lambda_N$to $x = \lambda_P$. The cation-exchange layer has a negative fixed charge concentration X_N and lies from $x = -d_L$ to $x = 0$. The anion-exchange layer extends from $x = 0$ to $x = d_R$ and carries a positive fixed charge concentration X_P. Both X_N and X_P are assumed to be uniform in each layer. In Fig. 1, c_{iK} stands for the concentration of the ith ionic species in region K ($i = 1$ for the salt cation, $i = 2$ for the salt anion, $i = 3$ for the H^+ ion and $i = 4$ for the OH^- ion, with K = L for the left solution, K = N for the layer with negatively charged groups, K = P for the layer with positively charged groups and K = R for the right solution). The membrane system incorporates two diffusion boundary layers (DBLs) of thickness δ flanking the BM. Even when vigorous stirring is applied, the presence of these layers cannot be neglected [4,15]. In Fig. 1, $\Delta\psi_{DL}$, $\Delta\psi_{DJ}$, and $\Delta\psi_{DR}$ are the dimensionless Donnan potentials at the interfaces $x = -d_L$, $x = 0$ and $x = d_R$, respectively, and $\Delta\psi_L$, $\Delta\psi_R$, $\Delta\psi_N$, and $\Delta\psi_P$ are the dimensionless diffusion potentials in the bulk of the left and right DBLs, and in the ion-exchange layers N and P, respectively. All electric potential differences are calculated as left minus right potential values.

Improving the ionic selectivity of the membranes in such a way that the mechanical strength and chemical stability

* Corresponding author. Fax: +34963983385.
E-mail address: smafe@uv.es (S. Mafé).

PII: S0032-3861(99)00886-1

are not compromised is crucial in most practical applications [8,9,11,13]. This can be done only through a basic understanding of the physico-chemical phenomena involved. The electrochemical characterisation of BMs can be carried out by means of membrane potential [15,16] and current–voltage (*I–V*) [2–5,7,17] measurements. These experimental techniques provide valuable information about the functional and structural characteristics of the membranes [4]. In this work, we have studied theoretically and experimentally the influence of factors such as the bipolar junction structure, fixed charge concentration and preparation procedure on the ion selectivity and water dissociation rate of six commercial BMs.

2. Experimental

2.1. Membranes

Six different BMs were used: two of them, denoted as FTBM1 (FhIGB in previous studies) and FTBM2, from FuMA-Tech GmbH (St. Ingbert, Germany); one (denoted as WSI) from WSI Technologies Inc. (St. Louis, Missouri, USA); one Neosepta BP-1 (denoted as BP1) from Tokuyama Co. (Tokuyama, Japan); one Aqualytics BP6 (denoted as AP6) from Graver Water Company (New Jersey, USA); and one commercial BM (denoted as MB3) from Izd. NIITEKhIM (Moscow, Russia).

The FTBM1 membrane has a multilayered sandwich structure composed of a cation selective layer (sulfonic acid groups in a cross-linked sulfonated polytherketone), an anion selective layer (quaternary ammonium ions incorporated into a polysulfone matrix) and a very thin intermediate layer (about 10 nm thick) of an insoluble polyelectrolyte complex containing tertiary ammonium groups. This layer was inserted between the two ion-exchange layers in order to improve the water dissociation capability of the BM. The thicknesses of the layers are approximately 40 mm (cation-exchange layer) and 20 mm (anion-exchange layer) [7,8]. The FTBM2 membrane is identical to the FTBM1 except for the fact that the finished membrane is not reinforced by an inert polymer screen.

The WSI is a non-reinforced membrane consisting of two separate layers, which have to be laminated together by hand to form the bipolar structure [17]. The anion and cation-exchange layers contain, respectively, strongly basic quaternary ammonium groups and sulfonic acid groups as fixed charges. Both layers are Pall Rai films consisting of a fluorocarbon polymer matrix in which functional groups have been introduced by radiation grafting. If both layers remain together for a long time, water dissociation capability may decrease because of the accumulation of gas at the interface, what must be avoided separating both layers periodically or working in an environment where carbon dioxide is excluded [18]. The thickness of the anion-exchange layer is ca. 43 mm, and the thickness of the cation-exchange layer is ca. 73 mm [17].

The BP1 membrane is a reinforced BM obtained by comprising a cation-exchange membrane (with sulfonic acid groups) closely adhered to an anion-exchange membrane (with quaternary ammonium groups). The cation-exchange groups present at the adhered surface of the membrane have been exchanged with heavy metal ions, specially iron (II, III), ruthenium (III) and tin (II, IV) [19]. The AP6 membrane has an integrated multilayered structure based on a polystyrene matrix to which quaternary ammonium and sulphonic groups are attached [20]. The MB3 is a commercial membrane that has a bilayer sandwich structure, containing phosphoric acid groups in the cation-exchange layer and quaternary ammonium groups in the anion-exchange layer [21,22].

2.2. Membrane potential

The experimental setup used to measure the membrane potential of the BMs is shown schematically in Fig. 2. The measuring cell is composed of two coaxial cylindrical compartments with different radii, so that the inside compartment contains the reference concentration (1 M KCl) solution, and the outside one holds the variable KCl solution whose concentration was varied between 10^{-3} and 2 M. The conductivity of the solutions is controlled during the measurements in order to avoid contamination effects in very dilute solutions. Two magnetic stirrers are used, one located in the outside solution just under the membrane and the other in the inside solution over the membrane, with the idea of minimising the thickness of the (unstirred) DBLs formed on the membrane–solution interfaces [15]. The membrane potential is measured using two calomel electrodes [23]. Each experimental membrane potential value is not accepted until steady state conditions are reached. As it was shown in previous studies on membrane potential of BMs [15], the time necessary to attain steady-state conditions reduces considerably as stirring rates increase. All measurements were performed at room temperature (298 K).

2.3. Current–voltage curves

The *I–V* curves under forward and reverse electrical polarisation are obtained using a four-point measuring technique [24] with a conical-shaped cell designed to minimise border effects and make approximately homogeneous the current through the membrane (see Fig. 3). The BM of cross-section area $A = 0.20\ \mathrm{cm}^2$ is placed between the two electrodialytic halves of the cell, and fixed with a thin rubber ring, so that the membrane does not move during measurements. The whole cell is filled with 0.5 M KCl aqueous solution and the membrane is allowed to equilibrate for several hours with the same solution used in the experiment before each set of measurements. The solution is pumped into the cell, and the stream directed to the

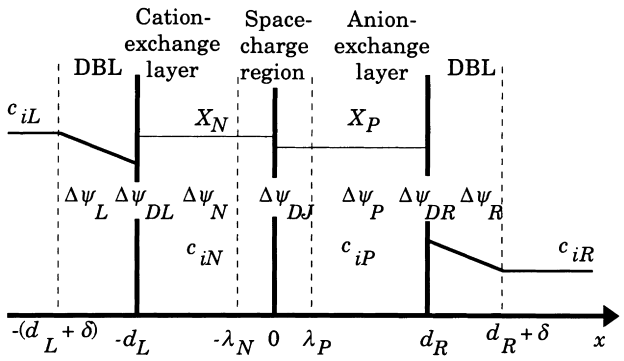

Fig. 1. Schematic view of the BM system. The space charge region between $x = -\lambda_N$ and $x = \lambda_P$ corresponds to the bipolar junction. The symbols denote the ion concentrations and the dimensionless electric potential drops in the different regions, and are defined in the text. We have incorporated two DBLs of thickness δ adjacent to the membrane/solution interfaces.

membrane surface so that no additional stirring is necessary during the experiments. As soon as both streams leave each corresponding half, they are mixed, and the pH value of the whole solution is maintained constant. The current is introduced by two Ag/AgCl plates (whose diameter is ca. 3.1 cm) prepared electrolysing a silver plate as an anode in 0.1 M HCl aqueous solution with an electric current of 1 mA. The potential is measured by means of two Haber–Luggin capillaries (HLC) filled with a 3 M KCl saturated solution as a salt bridge. They are located in front of each membrane surface, at 1.5 mm approximately (see Fig. 3). The potentiostat is controlled by a computer, so that each experimental point is not accepted until the fluctuations in the measured value are lower than a prefixed tolerance level. The temperature is controlled by a thermostated coiled glass heat exchanger placed between the solution reservoir and the cell. Temperature measurements are made in the solution reservoir and inside the cell, trying to avoid thermal gradients during the experiments.

3. Results

In this section, we present the experimental membrane potential and *I–V* curves obtained for the six BMs described in the previous section.

The membrane potential is defined as the potential difference appearing between the two solutions flanking the membrane when these solutions contain the same electrolyte at different concentrations and there is no current flow. The magnitude and sign of the potential depends then on the nature of the membrane and the permeating species [15,16,25]. The results of membrane potential $\Delta\phi_M$ (defined as left minus right potential values in Fig. 1) vs $\log_{10}(c_R/c_L)$ for the BMs are shown in Fig. 4. For all membranes $\Delta\phi_M$ increases as the concentration ratio decreases from unity. This effect is specially noticeable in the BP1 membrane, which attains values as high as 180 mV when $(c_R/c_L) = 10^{-3}$. Note also the significant differences found between the FTBM1 and FTBM2 membranes, that could be ascribed to the reinforcing material present in the FTBM1 membrane. Indeed, membrane FTBM2 lacks this inert material, and then the fixed charge groups attached to the membrane polymer chains are responsible for the osmotic pressure that gives rise to membrane swelling. This swelling is prevented by the reinforcing material in membrane FTMB1. The higher the membrane swelling, the lower the ionic selectivity due to the fixed charges and, therefore, the lower the membrane potential [23].

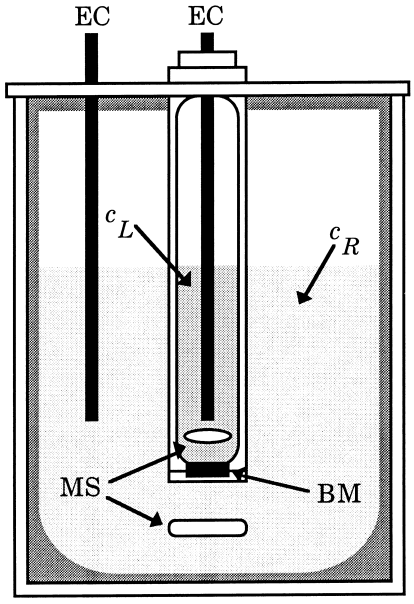

Fig. 2. Sketch of the experimental setup used to measure membrane potential of BMs. EC denotes the calomel electrodes, c_L and c_R refer, respectively, to the concentrations of the left (reference) and right (variable) solutions of Fig. 1, and MS are the magnetic stirrers.

The experimental *I–V* curves obtained for the BMs are shown in Fig. 5. The curves show the typical behaviour given by the coupling of ion transport and EFE water dissociation BMs [4,26]: under forward polarisation ($V > 0$) the current is carried by the salt ions and increases rapidly with the applied voltage. The membrane shows then very low resistance values. For small reverse voltages ($V < 0$), the current is also carried mainly by the salt ions and attains a limiting value. The resistance of the membrane is then very large. At high reverse voltages, most of the current is carried by the H^+ and OH^- ions generated by the EFE water dissociation taking place at the bipolar junction, and increases rapidly with the voltage. The membrane resistance then begins to decrease again with the applied voltage.

Despite this common general behaviour, Fig. 5 shows that the particular characteristics of each curve depends strongly on the membrane considered. Two main factors appear to determine crucially the behaviour of BMs. Firstly, the structure of the bipolar junction between the two ion-exchange layers [3,4,6,27] and, secondly, the nature of the charged groups attached to the polymeric matrix [4,7,8,28]. Also,

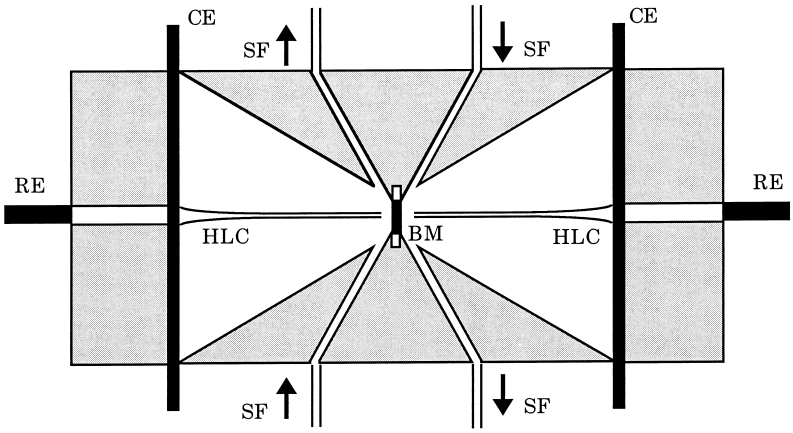

Fig. 3. Experimental setup of the four-point measuring cell employed for the *I–V* curves. Two Ag/AgCl plates are used as current electrodes (CE), and the potential across the BM is measured with two reference electrodes (RE) using Haber–Luggin capillaries (HLC) as salt bridges. The solution flux (SF) is directed to the membrane and mixed up to keep constant the pH and temperature solution values.

even when two different samples of the same membrane are compared, it is still possible to find some differences between them due to the sensitivity of the *I–V* curves to the particular membrane characteristics.

4. Discussion

We will now discuss the experimental results of the previous section, making use of a theoretical model for the BM.

The theoretical model for the membrane potential is based on the Nernst–Planck equations, and can be considered as an extension of the TMS theory [15,23,25]. This theory ascribes the ion selectivity to the presence of fixed charges attached to the membrane chains. It gives the ion fluxes and potential differences across the membrane on the basis of the Donnan equilibrium assumption at the membrane/solution interface and the Nernst–Planck flux equation [23,25]. The TMS theory assumes further that the transport process is controlled entirely by the membrane. Extensions of this theory to the case of ion-exchange bipolar membranes have been given recently, and details can be found in Refs. [15,29].

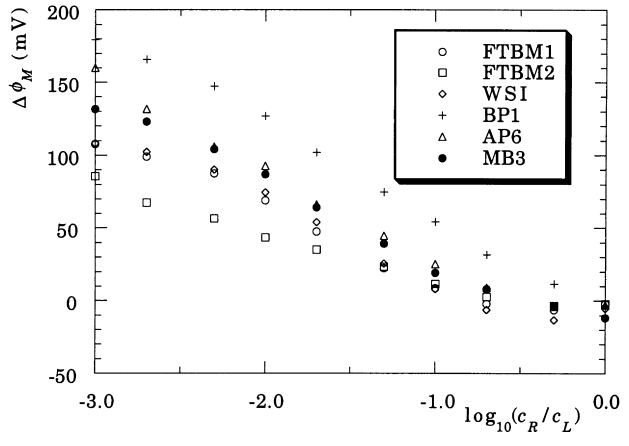

Fig. 4. Experimental values of membrane potential vs $\log_{10}(c_R/c_L)$ with the reference concentration $c_L = 1$ M KCl for the six BMs under study. All measurements were carried out at $T = 298$ K. Concentrations c_L and c_R correspond to the inside (reference) and outside (variable) solutions of Figs. 1 and 2, respectively.

In order to understand qualitatively the experimental data shown in Fig. 4, we assume that the main contributions to the membrane potential arise from the potential drops at the three membrane interfaces. In the symmetrical case the ion-exchange layer thicknesses are $d_L = d_R \equiv d$, the ion diffusion coefficients are $D_{iK} \equiv D_S$ (the same for both salt ions) and the fixed charge concentrations are $X_K \equiv X(i = 1, 2, K = N, P)$. Then, the membrane potential is:

$$\Delta\phi_M \approx \frac{RT}{F}(\Delta\psi_{DL} + \Delta\psi_{DJ} + \Delta\psi_{DR})$$

$$\approx \frac{RT}{F}\left[\ln\frac{\sqrt{1+v_L^2}+1}{v_L} + \ln\frac{y-1}{y+1} + \ln\frac{v_R}{\sqrt{1+v_R^2}-1}\right] \quad (1)$$

where

$$v_i \equiv 2c_i/X, \qquad i = L, R \quad (2)$$

and

$$y \equiv \frac{\sqrt{1+v_L^2}+\sqrt{1+v_R^2}}{2} \quad (3)$$

In Eq. (1) constants F, R, and T have their usual meaning [15]. Fig. 6 shows the membrane potential vs $\log_{10}(c_R/c_L)$ values calculated from Eq. (1) using $c_L = 1$ M and $d = 10^{-4}$ m. The curves are parametric in the fixed charge concentration. Comparison of Figs. 4 and 6 shows that the higher membrane potential values correspond to the BMs having the higher fixed charge concentrations. The BP1 membrane presents the highest membrane potential, while

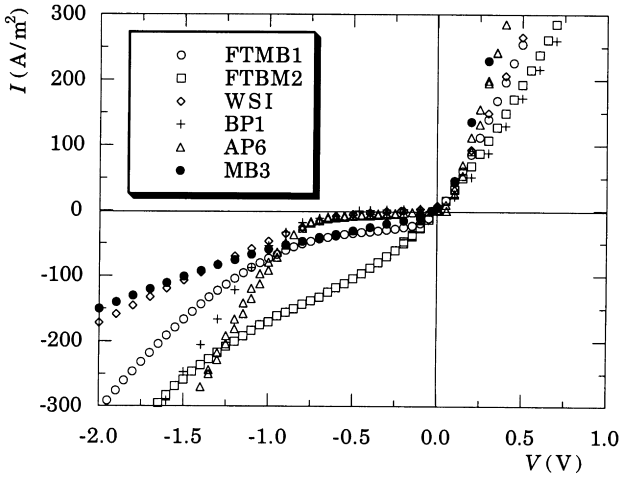

Fig. 5. Experimental *I–V* curves obtained for the six BMs in an aqueous solution of $c_S = 0.5$ M KCl. All measurements were carried out at $T = 298$ K.

the FTBM2 membrane reaches values about 50% smaller. The rest of the BMs exhibit similar behaviour despite the fact that they have very different bipolar junction structures (WSI is a bilayer, MB3 is a sandwich-type membrane and the other ones are all monolayers). This result indicates that the membrane potential (and then the ionic selectivity) depends significantly on the bulk characteristics of the ion-exchange layers. Also, the comparison between FTBM1 and FTBM2 membranes confirms the effect mentioned in the previous section: the lack of reinforcing material causes a significant swelling of the FTBM2 membrane and thus its effective fixed charge concentration becomes significantly lower than that of the (reinforced) FTBM1 membrane (see Figs. 4 and 6).

The experimental points in Fig. 4 however show some disagreement with the simple model described in Eqs. (1)–(3): membranes WSI, FTBM1 and MB3 attain a minimum

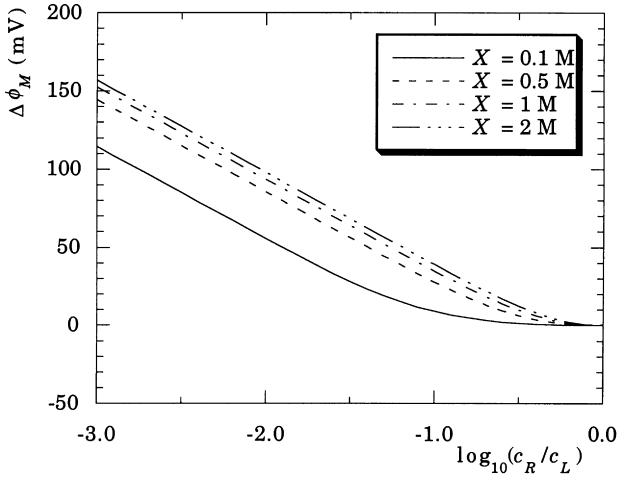

Fig. 6. Calculated membrane potential vs $\log_{10}(c_R/c_L)$ with $c_L = 1$ M in Eq. (1). The curves are parametric in the fixed charge concentration.

at $c_R/c_L < 1$. The position of the minima in these curves should be ascribed to a departure from the symmetrical BM assumption $d_L = d_R$, $D_{iK} \equiv D_S$ and $X_K \equiv X (i = 1, 2,\ K = N, P)$ introduced in Eq. (1) [15].

It can also be noted that for very dilute solutions ($10^{-3} < c_R/c_L < 10^{-2}$) an inflection point not anticipated in the above theory appears in the experimental curves. This can be explained taking into account the contribution of the DBLs to the membrane potential (see Fig. 7). Indeed, comparison between the calculated values with ($\delta \approx 0$) and without ($\delta \neq 0$) stirring shows significant differences due to the change in the hydrodynamic conditions of the unstirred DBLs. The contribution of the DBLs to the observed membrane potential increases with the magnitude of the salt flux through the system, and is not negligible for dilute solutions [15].

The experimental behaviour of the *I–V* curves shown in Fig. 6 can also be discussed in terms of a previous theoretical model [4,29] based on the Nernst–Planck flux equations. In the most general case, these equations cannot be integrated in a closed form. Nevertheless, approximate solutions can be derived under appropriate simplifying assumptions.

For forward and small reverse voltages, most of the current is carried by the salt ions, and therefore the contribution of water ions can be neglected. In the symmetrical case $d_L = d_R \equiv d$, $X_N = X_P \equiv X$, $D_{iK} \equiv D_S (i = 1, 2;\ K = N, P)$, $c_{iK} \equiv c_S (i = 1, 2;\ K = L, R)$, the *I–V* curve can be expressed in the form [29]

$$FV/RT = \ln \frac{\sqrt{X^2 + 4c_S^2} + X}{\sqrt{X^2 + 4c_S^2} - X} + \ln \frac{\sqrt{X^2 + 4c_S^2 + 2XdI/D_S F} - X}{\sqrt{X^2 + 4c_S^2 + 2XdI/D_S F} + X} + \frac{2}{X}\left[\sqrt{X^2 + 4c_S^2 + 2XdI/D_S F} - \sqrt{X^2 + 4c_S^2}\right] \quad (4)$$

In Eq. (4), the first term accounts for the Donnan voltage drops at the membrane/solution interfaces, the second one for the voltage drop at the inner membrane interface, and the third one for the voltage drops across the bulk of the ion-exchange layers. Fig. 8 shows the *I–V* curves obtained from Eq. (4) using the typical parameters $d = 100$ μm, $D_S = 10^{-6}$ cm²/s, $c_S = 0.5$ M and different values of the fixed charge concentration. Comparison of Figs. 5 and 8 permits one to obtain some conclusions concerning the ionic selectivity of BMs. The low limiting currents measured in Fig. 5 for $V < 0$ indicate that all membranes (except FTBM2) present relatively high fixed charge concentrations (see Eq. (4)). This fact becomes crucial in practical applications, where high selectivities are required in order to avoid the current leakage and the salt back diffusion [7,8]. Note also that the ionic selectivity scale deduced from the limiting

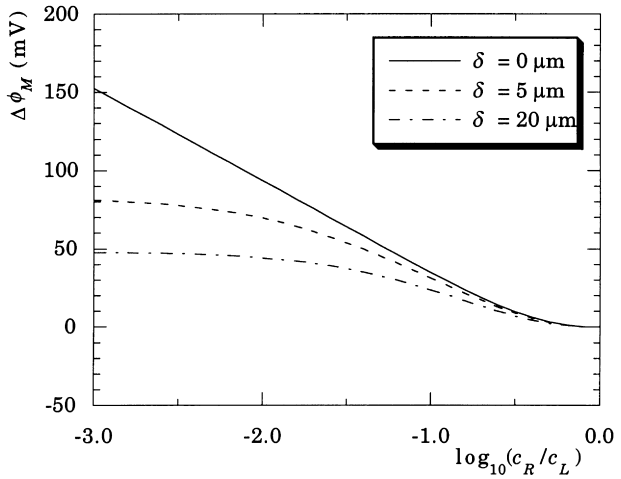

Fig. 7. Calculated membrane potential vs $\log_{10}(c_R/c_L)$ with $c_L = 1$ M and $X = 1$ M. The curves are parametric in the DBL thickness δ, and are now calculated taking into account the contribution of the DBLs to the membrane potential [15].

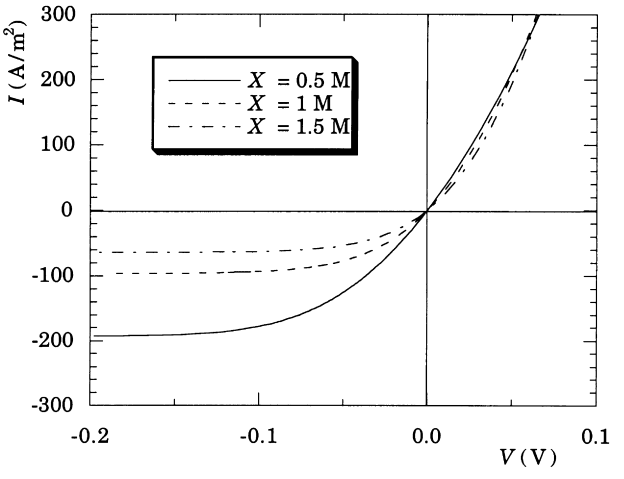

Fig. 8. Theoretical *I–V* plots for forward ($V > 0$) and low reverse ($V < 0$) polarisation calculated from Eq. (4). The curves are parametric in the fixed charge concentration $X_N = X_P \equiv X$ of the BM.

currents of Fig. 5 (a low limiting current corresponds to a high ionic selectivity) is approximately the same compared to that obtained from membrane potential measurements in Fig. 4 (a high membrane potential corresponds to a high ionic selectivity).

The experimental trends observed under forward polarisation also agree with the theoretical predictions: the rapid increase of the electric current with the applied potential for $V > 0$ is common to Figs. 5 and 8. However, the measured voltage drops under forward polarisation are significantly higher than the theoretical predictions. This can be explained taking into account the fact that the voltage drops across the membranes have been measured placing two capillaries in the surrounding solutions. Under forward polarisation, the BMs offer a very low resistance, so that the ohmic voltage drops in the solution layers between the membrane and the capillaries must be considered together with Eq. (4) in order to account for the experimental results. Note that in reverse polarisation ($V < 0$) this effect is not so important because the resistance of the BM is considerably higher in this case.

Moreover, the measurements taken under forward polarisation present additional difficulties: at high enough electric currents, hydrated ions accumulate at the bipolar junction, and a growing solution layer appears between the two layers of the BM. The presence of this layer modifies the structure of the bipolar junction and increases the electrical resistance of the whole system. Nevertheless, since these factors should affect all the membranes in a similar way, the above arguments explaining the behaviour of the membranes under forward polarisation and (small) reverse polarisation remain essentially valid.

In the case of high reverse voltages, most of the current is carried by the H^+ and OH^- ions and, therefore, the *I–V* characteristics are dictated by the capability of each membrane to produce these ions. The experimental trends observed in Fig. 5 can be discussed in terms of a theoretical model based on the Nernst–Planck and Poisson equations [3,4]. At high enough reverse polarisation, and for the symmetrical case $d_L = d_R \equiv d$, $X_N = X_P \equiv X$, $D_{iK} \equiv D_S (i = 1, 2;\ K = N, P)$, $D_{iK} \equiv D_W (i = 3, 4;\ K = N, P)$, $c_{iK} \equiv c_S (i = 1, 2;\ K = L, R)$, $c_{iK} \equiv c_W (i = 3, 4;\ K = L, R)$, the *I–V* curve can be expressed in the form [4]

$$I = (I_{LS} + I_{LW})[\exp(FV/RT) - 1] - I_d \tag{5}$$

In Eq. (5) I_d accounts for the current density carried by the H^+ and OH^-. These ions are generated by the EFE protonation–deprotonation reactions between the fixed charge groups and the water molecules occurring at the bipolar junction. The I_d term can be written as [3,4]

$$I_d \approx F k_d^0 \exp\left[\frac{\alpha F}{RT} E\right] n\lambda \tag{6}$$

where k_d^0 stands for the net rate dissociation constant of the reactions when no external electric field E is applied, n is the concentration of active sites where the reactions are taking place, α is a reaction distance [6,30], and

$$E \equiv \sqrt{\frac{FX}{\epsilon_r \epsilon_0}(-V)} \tag{7a}$$

$$\lambda \equiv \sqrt{\frac{4\epsilon_r \epsilon_0}{FX}(-V)} \tag{7b}$$

are, respectively, the maximum electric field at the bipolar junction and the length of the space charge region in the junction [4]. In Eqs. (7a) and (7b), $\epsilon_r \epsilon_0$ is the electrical permittivity of the bipolar junction.

In Eq. (5) I_{LS} and I_{LW} refer to the limiting currents for salt and water ions, respectively, and are defined in the form

$$I_{LS} \equiv 2FD_S c_{2N}(-d)/d \tag{8a}$$

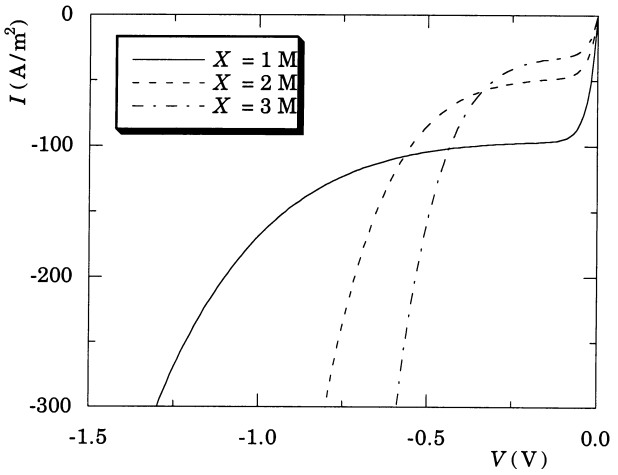

Fig. 9. Theoretical *I–V* plots for reverse ($V < 0$) polarisation calculated from Eq. (5). The curves are parametric in the fixed charge concentration $X_N = X_P \equiv X$.

$$I_{LW} \equiv 2FD_W c_{4N}(-d)\sqrt{k_r^0 c_{3N}(-d)/D_W}\,\coth(\sqrt{k_r^0 c_{3N}(-d)/D_W}) \tag{8b}$$

where

$$c_{iN}(-d) = \frac{c_{iL}}{c_{1L} + c_{3L}}[\sqrt{X^2/4 + (c_{1L} + c_{3L})^2} + (-1)^{i+1}X/2],$$

$$i = 1,\ldots,4 \tag{9}$$

according to the Donnan equilibrium [23] and k_r^0 is the rate constant for recombination.

Since I_d depends exponentially on E [4,30], this term increases rapidly with the reverse voltage, and prevails then over the other terms in Eq. (5) for $V < 0$. In addition, I_d depends on both the nature of the active groups (via k_d^0 and n) and the structure of the space charge region where the reaction is taking place (via E and λ). These results can be seen in Fig. 9, where the theoretical *I–V* curves correspond to the typical values $d = 50$ μm, $D_S = 10^{-6}$ cm^2/s, $D_W = 10^{-5}$ cm^2/s, $c_{iK} \equiv c_S = 0.5$ M ($i = 1,2$; K = L, R), $c_{iK} \equiv c_W = 10^{-7}$ M, ($i = 3,4$; K = L, R), $\epsilon_r = 25$, $k_d^0 n = 400$ mol/m^{3}s, $k_r^0 = 1.11 \times 10^{11}$ M^{-1}s^{-1}, $\alpha = 2.5$ Å and $T = 298$ K. The curves of Fig. 9 are parametric in the fixed charge concentration: $X = 1$ M (continuous line), $X = 2$ M (dashed line) and $X = 3$ M (dotted–dashed line). They are in qualitative agreement with the experimental results observed in Fig. 5, where each BM shows different *I–V* characteristics for $V < 0$. Membranes BP1, AP6 and FTBM1 appear to be significantly more efficient than the others in the production of H^+ and OH^- ions. This fact suggests that the local properties of the junction exert a decisive influence on the water dissociation. Note that the resistance of the interfacial layer is expected to be higher in bilayer (WSI) and sandwich-type (MB3) BMs than in the monolayer BMs where the thickness of the junction is smaller. However, the presence of catalytic agents that enhance the water dissociation at the bipolar junction should also be important here.

Once again, the comparison between membranes FTBM1 and FTBM2 reveals some of the physical mechanisms involved. Although FTBM1 has a higher ionic selectivity than FTBM2, the two membranes show similar efficiency in the production of H^+ and OH^- ions at high enough reverse polarisation voltages. This fact suggests that the active layer inserted between the ion-exchange layers of the two membranes is the main responsible for the water dissociation capability. Thus, the lack of reinforcing becomes apparent as a bulk effect that determines the ionic selectivity of the BM, but it does not appear to affect the performance of the bipolar junction where the water dissociation reactions take place.

To sum up, we have shown that the two main factors determining the performance of polymer BMs in practical applications, the ion selectivity and the water dissociation rate, can be studied by means of membrane potential and *I–V* measurements. The qualitative agreement found between theory and experiments allows a better understanding of the BM behaviour and demonstrates that not only the structure of the bipolar junction but also the bulk properties of the two ion-exchange layers are important in practical applications.

Acknowledgements

Financial support from the European Union (Brite-Euram III, Thematic Network No. BRRT-CT97-5038), Fundació UJI-Bancaixa (Project No P1B98-12) and DGICYT, Ministry of Education and Science of Spain (Project No PB98-0419) are gratefully acknowledged.

References

[1] Simons R. Electrochim Acta 1984;29:151.
[2] Zabolotskii VI, Shel'deshov NV, Gnusin NP. Russ Chem Rev 1988;57:801 (Uspekhi Khimii, 1988;57:1403).
[3] Ramírez P, Rapp HJ, Mafé S, Bauer B. J Electroanal Chem 1994;375:101.
[4] Mafé S, Ramírez P. Acta Polym 1997;48:234.
[5] Shimizu K, Tanioka A. Polymer 1996;38:5441.
[6] Mafé S, Ramírez P, Alcaraz A. Chem Phys Lett 1998;294:406.
[7] Strahmann H, Rapp HJ, Bauer B, Bell CM. Desalination 1993;90:303.
[8] Strahmann H, Bauer B, Rapp HJ. Chemtech 1993;June:17.
[9] Graillon S, Persin F, Pourcelly G, Gavach C. Desalination 1996;107:159.
[10] Thompson R, Paleologou M, Berry RM. Tappi J 1997;80:154.
[11] Alvarez F, Alvarez R, Coca J, Sandeaux J, Sandeaux R, Gavach C. J Membr Sci 1997;123:61.
[12] Bazinet L, Lamarche F, Labrecque R, Ippersiel D. J Agric Food Chem 1997;45:3788.
[13] Bazinet L, Lamarche F, Ippersiel D. J Agric Food Chem 1998;46:2013.
[14] Tronc S, Lamarche F, Makhlouf J. J Agric Food Chem 1998;46:829.
[15] Ramírez P, Mafé S, Manzanares JA, Pellicer J. J Electroanal Chem 1996;404:187.

[16] Higa M, Kira K. J Phys Chem 1995;99:5089.
[17] Simons R. J Membr Sci 1993;78:13.
[18] Simons R. Bipolar membrane and method for its preparation. Australian Patent, PCT/AU90/00241.
[19] Hanada F, Hiraya K, Ohmura N, Tanaka S. Tokuyama Soda Kabushiki Kaisha. Bipolar membrane and method for its production. European patent, No. 0 459 820 A2.
[20] http://www.aqualytics.com.
[21] NIITEKhIM. Ion exchange membranes, granular materials and powders. (Catalogue). Izd NIITEKhIM, Moscow, 1977.
[22] Zabolotskii VI, Sheldeshov NV, Gnusin NP. Sov Electrochem 1987;22:1573 (Élektrokhimiya, 1986;22:1676).
[23] Helfferich F. Ion exchange. New York: McGraw-Hill, 1962.
[24] Holdik H, Alcaraz A, Ramírez P, Mafé S. J Electroanal Chem 1998;442:13.
[25] Lakshminarayanaiah N. Transport phenomena in membranes. New York: Academic Press, 1969.
[26] Ramírez P, Rapp HJ, Reichle S, Strathmann H, Mafé S. J Appl Phys 1992;72:259.
[27] Mauro A. Biophys J 1962;2:179.
[28] Krol JJ. Monopolar and bipolar ion exchange membranes. Mass transport limitations. PhD thesis. University of Twente, 1997.
[29] Sokirko AV, Ramírez P, Manzanares JA, Mafé S. Ber Bunsenges Phys Chem 1993;97:1040.
[30] Timashev SF, Kirganova EV. Sov Electrochem 1982;17:366 (Élektrokhimiya, 1981;17:440).